Crystal-Facet-Dependent Metallization in Electrolyte-Gated Rutile TiO_2 Single Crystals

Thomas D. Schladt,[†] Tanja Graf,[†] Nagaphani B. Aetukuri,[†,‡] Mingyang Li,[†,§] Andrea Fantini,[†] Xin Jiang,[†] Mahesh G. Samant,[†] and Stuart S. P. Parkin[†,*]

[†]IBM Almaden Research Center, San Jose, California 95120, United States and [‡]Department of Materials Science and Engineering and [§]Department of Physics, Stanford University, Stanford, California 94305, United States

ABSTRACT The electric-field-induced metallization of insulating oxides is a powerful means of exploring and creating exotic electronic states. Here we show by the use of ionic liquid gating that two distinct facets of rutile TiO_2, namely, (101) and (001), show clear evidence of metallization, with a disorder-induced metal—insulator transition at low temperatures, whereas two other facets, (110) and (100), show no substantial effects. This facet-dependent metallization can be correlated with the surface energy of the respective crystal facet and, thus, is consistent with oxygen vacancy formation and diffusion that results from the electric fields generated within the electric double layers at the ionic liquid/TiO_2 interface. These effects take place at even relatively modest gate voltages.

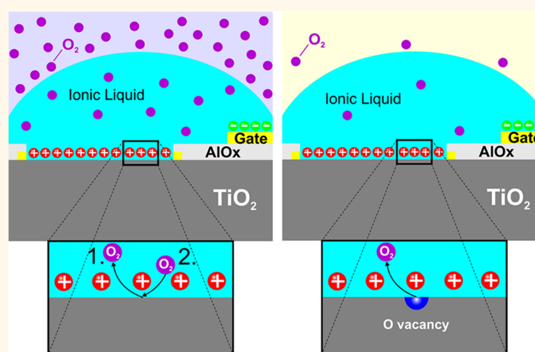

KEYWORDS: electrolyte gating · titanium dioxide · metallization · disorder-induced metal—insulator transition · oxygen vacancy formation · crystal facet dependence

The possibility of using electric fields to modify the electronic and transport properties of semiconducting and insulating materials has a decades long history and forms the technological basis for silicon microelectronics.[1,2] Electric fields can be applied in various ways including internally generated fields at electronically mismatched interfaces, such as Schottky barriers[2] and polar discontinuities,[3] and in field effect transistor devices using gates formed from conventional and high *k* dielectrics or ferroelectric materials.[1] Of particular interest are conducting layers created at the interface between nominally insulating oxides, such as those found in sandwiches of $SrTiO_3$ (STO) and $LaAlO_3$ (LAO)[3] and superlattices of STO and $GdTiO_3$ (GTO),[4] in which the polar nature of the (001)-oriented LAO and GTO surfaces, respectively, provides for large internal electric fields.[5,6] However, the electric fields are so high[7] that the possibility of atomic reconfigurations at the interface and motion of atoms and vacancies at and beyond the interface cannot be ruled out.[8−10] To achieve similarly high electric fields using conventional gate dielectrics is not possible but is readily achieved using ionic liquids as the gate material.[11−17] Moreover, this allows for the tunability of the electric field *via* gate voltage control of the electric double layer (EDL) that is formed at the oxide/ionic liquid interface and, furthermore, does not restrict the interface orientation, as is the case when polar surfaces are used to create high electric fields. Here we show that electrolyte gating of rutile TiO_2 gives rise to metallization that varies strongly with the TiO_2 crystal facet orientation and which can be correlated with the surface energy of the corresponding facet, providing strong evidence that the electric-field-induced conductance arises from the formation of oxygen vacancies, as has recently been demonstrated for electrolyte-gated VO_2 (001) epitaxial films.[18]

RESULTS

Dependence of Gating Response on Crystal Facet of TiO_2. Figure 1a shows a schematic diagram of the planar EDLT device configuration and measurement circuitry used in this study (see the Methods section and Supporting

* Address correspondence to stuart.parkin@us.ibm.com.

Received for review June 30, 2013 and accepted August 20, 2013.

Published online August 20, 2013
10.1021/nn403340d

© 2013 American Chemical Society

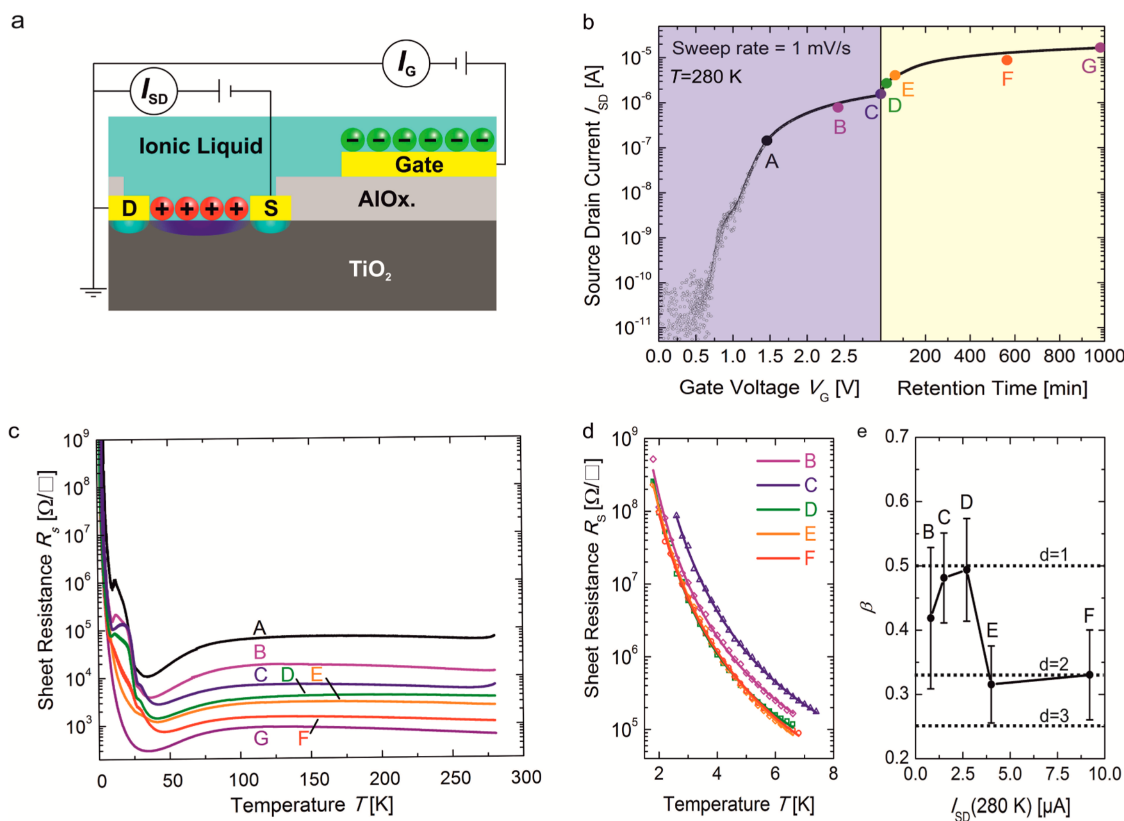

Figure 1. Electronic transport characteristics of a (101) TiO_2-based EDLT device. (a) Device schematic including the measurement circuit. (b) Typical transfer curve, I_{SD} *vs* V_G, as V_G is increased from 0 to 3 V for rutile (101) TiO_2 at 280 K, using a sweep rate of 1 mV s^{-1} and a V_{SD} of 0.1 V. After V_G = 3 V is reached, I_{SD} further increases over time, leading to $I_{SD} > 10\,\mu A$ after 1000 min. (c) Representative R_S-T curves for various I_{SD}. In the range of 35–45 K, the onset of localization of charge carriers leads to an increase in R_S by a factor of at least 10^5. (d) R_S *vs* T fitted with a variable-range hopping model at low temperatures with values of β shown in (e), as a function of the initial I_{SD} at 280 K. The data and fits are shown as symbols and solid lines, respectively. The dimensionality d corresponding to β is shown as dotted lines in (e). In (c–e), the letters indicate values of I_{SD} at 280 K approximately corresponding to points A–G indicated in (b).

Information for details on the device dimensions and fabrication). Typical device characteristics for a (101)-oriented rutile TiO_2 EDL transistor (EDLT) are shown in Figure 1b. The source–drain current I_{SD} is plotted as a function of the gate voltage V_G at a constant source–drain voltage V_{SD} = 100 mV using EMIM TFSI as the electrolyte. The devices are insulating for V_G = 0 V with an off-state current I_{SD} of less than 0.2 nA. However, a sharp increase in I_{SD} of more than 4 orders of magnitude is observed as V_G is ramped from 0 to 3 V. Moreover, I_{SD} continues to rise over time when V_G is maintained at 3 V, as shown on the right side of Figure 1b. Figure 1c displays the sheet resistance (R_S) of a (101) TiO_2 EDLT device as a function of temperature for various I_{SD} values measured at 280 K (indicated by points A–G in Figure 1b). Upon cooling, R_S increases slightly between 280 and 130 K. Below 130 K, R_S decreases and displays a minimal value in the range of 35–45 K. On further cooling, there is a metal–insulator transition and R_S increases abruptly by at least 5 orders of magnitude. We ascribe the dramatic increase of R_S at low temperatures to Anderson localization which is evidence for defect-induced disorder.[19] Consequently, we fit our low-temperature data using Mott's variable-range hopping model for which $R = R_0T^{2\beta}\exp(T_0/T)^{\beta}$, where $\beta = 1/(d+1)$ is a characteristic parameter for a d-dimensional system. Figure 1d shows that the low-temperature data are in excellent agreement with a variable-range hopping model over 4 orders of resistance change. Furthermore, the extracted β values from the fits, shown in Figure 1e, point to a 1D to 2D transition as a function of increasing carrier density. However, due to the large error bar in the extracted β values, it is difficult to conclude unambiguously that there is such a dimensionality change. Similar electronic transport characteristics have been reported for oxygen-deficient rutile TiO_2 and were attributed to multiple-band conduction.[20,21] This suggests that the electric-field-induced formation of oxygen vacancies in EDL devices might be responsible for their similar electrical transport characteristics.

Defect formation and migration at surfaces can be highly anisotropic with, in general, high surface energy crystal facets being more susceptible to defect formation. We, therefore, performed crystal-facet-dependent

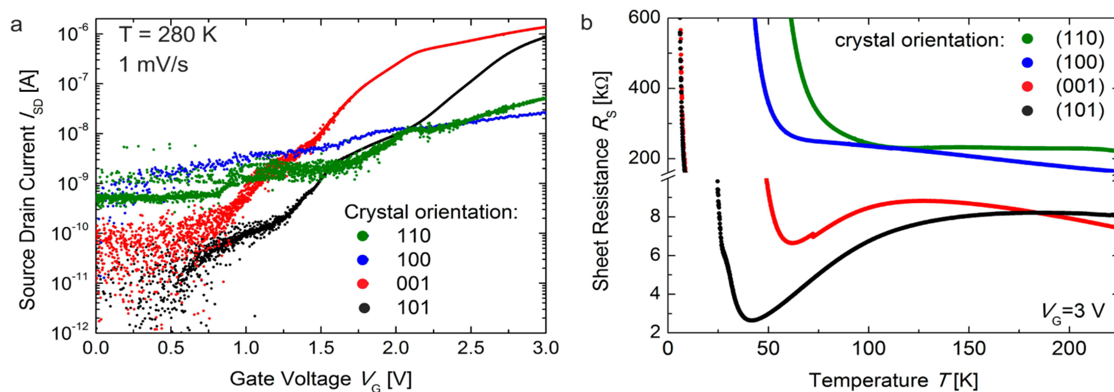

Figure 2. Crystal orientation dependence of the TiO_2-based EDLT characteristics. (a) I_{SD} as a function of V_G for four facets of TiO_2. V_G was ramped at 1 mV s^{-1} to 3 V at 280 K. (b) R_S *versus* temperature for V_G = 3 V measured at V_{SD} = 0.1 V for the same crystals.

EDL gating studies on four distinct facets of rutile TiO_2, namely, the (100), (001), (110), and (101) crystal facets. We find a remarkable dependence of the EDLT gating effect on the orientation of the rutile TiO_2 crystals, as shown in Figure 2a. While the channel current rises only gradually, by a factor of 10 and 100 for (110) and (100) facets, respectively, I_{SD} increases dramatically by 5 orders of magnitude for (101) and (001) facets upon ramping V_G from 0 to 3 V. Temperature-dependent R_S measurements of the four different crystal orientations for V_G = 3 V show that (110)- and (100)-oriented samples exhibit semiconducting behavior, whereas the (001) orientation displays a similar nontrivial R_S-T dependence as the (101) facet (see Figure 2b and Figure S4). The magnitude of the gating effect correlates well with the corresponding surface energies (in the absence of electric field) of the respective crystal facets of rutile TiO_2 which increase in the order $E_{surf}(110) < E_{surf}(100) < E_{surf}(101) < E_{surf}(001)$.[22,23] TiO_2 crystals with higher surface energy facets have a higher propensity to form defects, such as oxygen vacancies and Ti^{3+} interstitials, which both act as n-type dopants and generate localized defect states within the band gap.[24]

We note that the observed gating response is not related to the anisotropy in conductivity of the various facets that we measured. It was reported for reduced rutile TiO_2 single crystals[25] that the charge carrier mobility and conductivity are highest along the rutile *c*-axis, that is, the crystallographic [001] direction.[25] Therefore, the conductivity of both (110) and (100) facets for which the *c*-axis lies in plane should be higher than the conductivity of (001) and (101) facets for which the *c*-axis lies out of plane and partly out of plane, respectively. Although the off-state current in pristine samples at V_G = 0 V is consistent with the expected conductivity anisotropy, the very different gating responses are difficult to understand if they are purely electrostatic in origin. We, therefore, hypothesize that the devices fabricated on high-energy facets should be more easily addressable by EDL gating, giving rise to the stronger gating effects that we observe for these facets. However, the role of the very high electric fields in the EDL and their influence on aiding the formation of oxygen vacancies is poorly understood. For example, *ab initio* calculations of the oxygen vacancy formation energy have been performed only in the absence of external electric fields.[26]

The EDL gating process on TiO_2 is largely reproducible, as shown by the successive cycling of V_G in Figure 3a for TiO_2 (101) at 280 K using EMIM TFSI as the ionic liquid (IL). Cyclic $I_{SD}-V_G$ sweeps from 0 V to +2.3 V, to −2.3 V, and back to 0 V were recorded consecutively using a sweep rate of 5 mV s^{-1} and a 5 min wait between each cycle. A considerable hysteresis is evident which increases with V_G and decreasing ramp rate. The minor increases in the off-state current compared to the pristine sample in Figure 2a are likely due to possible training effects which occur after the sample has been gated several times. The observed hysteresis suggests that the gating effects that we find are not purely electrostatic in origin but, since the gate current I_G, shown in the lower part of Figure 3a, remains lower than 1 nA for the entire V_G regime, electrochemical reactions within the IL can be ruled out. However, electrochemical redox reactions occurring at the TiO_2 surface remain a distinct possibility. Indeed, the integrated value of the gate current over the entire time of the gating process is ∼400 nC (Figure 3a). This can account for the creation of $\sim 10^{16}$ oxygen vacancies/cm^2 consistent with the carrier densities inferred from Hall data (see Figure S3b). This is consistent with an electric-field-driven migration of oxygen from within the interior of the oxide into the IL.

Dependence of Gating Response on Ionic Liquid. It is reasonable to assume that the size and the arrangement of the electrolyte ions on the TiO_2 surface will influence the EDL formation and will therefore influence the EDL gating process. Hence, we performed cyclic $I_{SD}-V_G$ measurements to ±2 V on TiO_2 (101) with

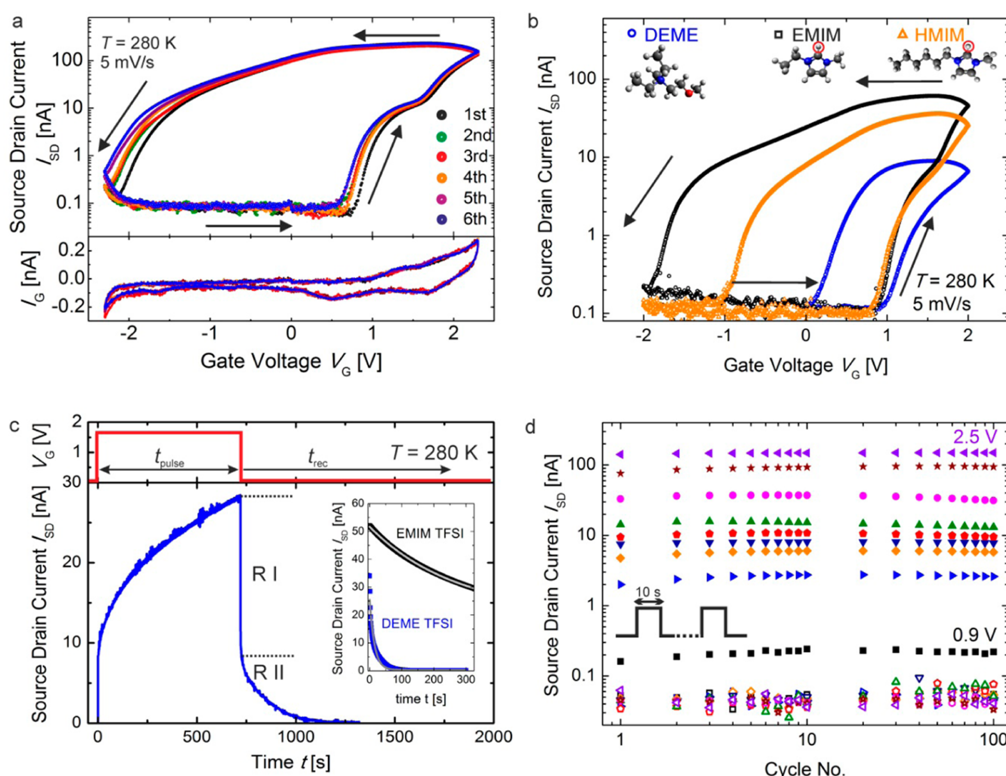

Figure 3. Dynamics of the (101) TiO_2-based EDLT. (a) Consecutive cycling of V_G between 0 to +2.3 V to −2.3 V and back to 0, recorded at 280 K with a sweep rate of 5 mV s^{-1} using EMIM TFSI as the electrolyte, with a waiting time of 5 min between consecutive cycles. The source−drain current I_{SD} and gate current I_G are shown in the top and bottom panels, respectively. The process is fully reproducible with only minor modifications in the observed hysteresis loops. (b) Cyclic V_G sweeps showing the influence of the electrolyte. When a non-imidazolium-based cation ($DEME^+$) is used, both the maximum I_{SD} and the I_{SD}−V_G hysteresis are reduced presumably due to a weaker interaction of the cation with the TiO_2 surface. The red circles highlight the acidic hydrogen atoms in the $EMIM^+$ and $HMIM^+$ molecules that likely form hydrogen bonds to oxygen atoms at the TiO_2 surface. Comparison of the imidazolium-based cations, $EMIM^+$ and $HMIM^+$, suggests that the bulkier nature of $HMIM^+$, due to its longer carbon side chain, leads to a lower affinity for surface attachment. (c) Response of I_{SD} to a single V_G pulse (1.75 V) with a duration time t_{pulse} = 720 s and the corresponding relaxation after the end of the pulse, using EMIM TFSI as the electrolyte, displaying a prolonged recovery with two distinct temporal regimes R I and R II. The inset compares the decay of I_{SD} in R II for EMIM TFSI with DEME TFSI. For optimal comparison, both experiments were performed on the same device after reaching a source−drain current of 90 nA. Solid lines indicate fits according to an exponential decay of I_{SD}. (d) Response of I_{SD} to V_G pulses of 10 s duration monitored for 100 cycles at 280 K (one cycle denotes V_G "ON" for 10 s followed by an "OFF" period of 10−60 s depending on the applied V_G). Shown are the "ON" (filled symbols) and "OFF" (open symbols) values of I_{SD} for V_G pulses ranging from 0.9 to 2.5 V in increments of 0.2 V. The I_{SD} response is stable, and the "OFF" currents are recovered for all gate voltages, demonstrating excellent reversibility for this range of V_G.

a ramp rate of 5 mV s^{-1} using ILs with coordinating imidazolium-based cations ($EMIM^+$ and $HMIM^+$) and noncoordinating ammonium-based cations ($DEME^+$) (see Figure 3b).[27,28] Several differences are apparent: first, the measured channel current at the highest gate voltage of V_G = 2 V is lowest for $DEME^+$ and highest for $EMIM^+$. Second, while a clear hysteresis is observed in all curves, the width of the hysteresis is largest for $EMIM^+$ and smallest for $DEME^+$ and, therefore, correlates with the magnitude of I_{SD}. It is possible that the higher binding affinity of imidazolium-based cations ($EMIM^+$ and $HMIM^+$) in combination with a stabilizing $\pi-\pi$ stacking interaction between neighboring imidazolium rings likely leads to a denser packing of the EDL[29,30] and a slower desorption of the chemisorbed cations, which is consistent, respectively, with a higher I_{SD} and a wider I_{SD}−V_G hysteresis. The high binding affinity is a result of a comparatively strong coordinative bond between the acidic H atom of the imidazolium ring to O atoms on the TiO_2 surface. The lower response of $HMIM^+$ compared to $EMIM^+$ could be due to a reduced surface coverage and a weaker hydrogen bond due to the bulkier nature of the $HMIM^+$ cations.[31] In contrast, $DEME^+$ as a quaternary ammonium ion possesses neither an imidazolium ring with a delocalized π-electron system nor an acidic H atom. Therefore, bonding of $DEME^+$ to the TiO_2 surface should be much weaker, and the packing density should be lower, resulting in a lower I_{SD} without hysteresis. However, the fact that the I_{SD}−V_G curves carried out with $DEME^+$ still exhibit considerable hysteresis suggests that, apart from the cation−TiO_2 interaction, slow relaxation and redistribution of accumulated defects within TiO_2 are important factors that will influence the dynamics of the EDL transistors, as we discuss below.

Time Dependence of Gating Response. Figure 3c shows the I_{SD} response to a V_G pulse of 1.75 V amplitude and

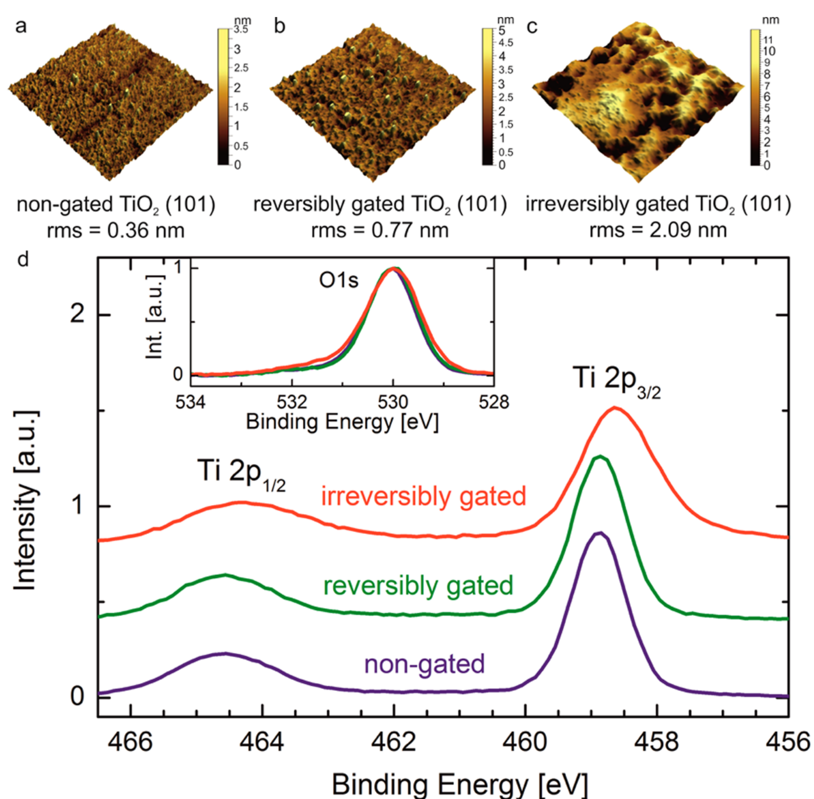

Figure 4. Surface defect formation on TiO_2 (101) by ionic liquid gating. The 1 μm × 1 μm AFM images of the (101) channel surface for (a) nongated, as-prepared device with rms roughness = 3.6 Å, (b) reversibly gated device with rms roughness = 7.7 Å, and (c) irreversibly damaged device with rms roughness = 20.9 Å. (d) Core-level XPS plots of the Ti 2p levels showing a shift of ∼0.2 eV toward lower energy after irreversible gating, consistent with a reduction of Ti^{4+}. There is no noticeable difference in the XPS spectra before and after reversible gating. The inset shows the O 1s peaks aligned to ∼530.1 eV.

720 s duration using EMIM TFSI as electrolyte. I_{SD} rises abruptly when V_G is turned "ON" but does not reach a saturation value by the end of the pulse. The rate of increase of I_{SD} with time during the pulse is steeper for higher gate voltages. We propose that a slow accumulation of oxygen vacancies results in the evolution and growth of a conducting path consisting of an oxygen-deficient TiO_{2-x} phase and, hence, a steady increase of I_{SD}.[32] The time scale of the recovery process depends on the magnitude of I_{SD} at the end of the pulse; for small currents, corresponding to low V_G and/or short pulses, I_{SD} returns to its "OFF" value within milliseconds, whereas for larger currents and/or longer pulses, a complete recovery is only achieved after several minutes. Furthermore, we observe two current decay regimes in the recovery process. We presume that the partial dissolution of the EDL is the rate-limiting step in the initial fast response regime (R I). Owing to the high ion mobility in the IL (∼10^{-3} cm^{-2} V^{-1} s^{-1}), the corresponding time constant is in the range of microseconds.[33,34] This initial regime is followed by a much slower regime (R II) which we speculate involves, on the one hand, desorption and diffusion of ions from the surface, which is again a consequence of the direct interaction between the IL molecules and the TiO_2 surface and, on the other hand, the repair and diffusion of defects within TiO_2 which were created during the gating step. This becomes even more apparent when the current decay is monitored for different ILs. The inset in Figure 3c shows the current decay of regime R II for the same device using EMIM TFSI and DEME TFSI as electrolytes obtained after I_{SD} was 90 nA. For DEME TFSI, the channel returns to its initial state within 60 s, whereas a complete recovery requires more than 10 min for EMIM TFSI, which is again consistent with a higher binding affinity of imidazolium-based cations at the surface of rutile TiO_2. Since the recovery time of 60 s for $DEME^+$ is too slow to be accounted for solely by ionic motion within the electrolyte, it rather indicates that the recovery of the initial insulating state is dominated by a slow redistribution of accumulated defects near the TiO_2 surface.

Figure 3d summarizes the dynamics of the switching behavior of TiO_2 (101) at 280 K in response to 100 V_G pulses of 10 s duration with amplitudes varying from 0.9 to 2.5 V. Filled symbols denote I_{SD} in the "ON" state, while open symbols show the corresponding "OFF" currents. The time period between two pulses was varied between 10 and 60 s to allow for a complete relaxation of the device. As can be seen, both "ON" and "OFF" state currents remain almost constant, indicating that no significant degradation of the device occurred upon repeated switching.

However, we observed that the gating effect was not completely reversible on (101)- and (001)-oriented samples if high gate voltages (>2.5 V) were applied for long periods of time; that is, the channel remained conducting after V_G was set to zero, whereas the initial state was always recovered for the (110) and (100) facets, respectively. To investigate possible surface modifications, we performed atomic force microscopy (AFM) on (101) channel surfaces in an as-prepared condition, after repeated reversible switching and after irreversibly gating by the application of high gate voltages (Figure 4a−c). The surface roughness already increases after reversible switching operations, supporting the hypothesized oxygen vacancy creation and migration. The irreversibly gated surface shows considerable damage that indicates a severe modification of the TiO_2 surface.

Oxidation State of Titanium from X-ray Photoelectron Spectroscopy. To further investigate the origin of this surface modification, we performed core-level X-ray photoelectron spectroscopy (XPS) analysis on the nongated, reversibly gated, and irreversibly gated samples within the channel region in each case after washing off the IL. We use the position of the O 1s peak (∼530.1 eV) to calibrate the binding energy.[35,36] For the reversibly gated sample, the XPS data (see Figure 4d) showed no shift in the binding energies of the Ti 2p and O 1s core-levels compared to the nongated sample. As expected, no change in the oxidation state of Ti was observed since the sample fully relaxed before the XPS measurement. Moreover, the binding energy difference (∼71.3 eV) between the O 1s and Ti $2p_{3/2}$ peaks is consistent with stoichiometric TiO_2.[35] After irreversible gating, however, the Ti $2p_{3/2}$ and Ti $2p_{1/2}$ peaks shift by ∼0.2 eV toward a lower binding energy with simultaneous broadening of these peaks, indicating that some Ti at the film surface has been reduced, consistent with oxygen vacancy creation and the damage to the surface observed in our AFM studies. On the basis of these results, we conclude that the surface damage on the reversibly gated device, as observed by AFM, is also caused by oxygen vacancy formation. However, the time scales for reoccupation of these vacancies are too short to trace a change in oxidation state by XPS.

Dependence of Gating Response on Presence of Oxygen. To provide further evidence for the role of oxygen vacancy formation in TiO_2, we performed EDL gating experiments in a pure oxygen atmosphere. Figure 5a shows the I_{SD} response of a 900 μm × 300 μm TiO_2 (101) device to a V_G = 2.5 V pulse for varying oxygen pressures p. We find that the response of TiO_2 crystals to gating by an EDL is suppressed in the presence of a sufficient pressure of oxygen supplied externally to the IL. Most importantly, we observed no I_{SD} response at V_G = 2.5 V when p = 120 mbar. However, I_{SD} increased significantly upon reducing the pressure to

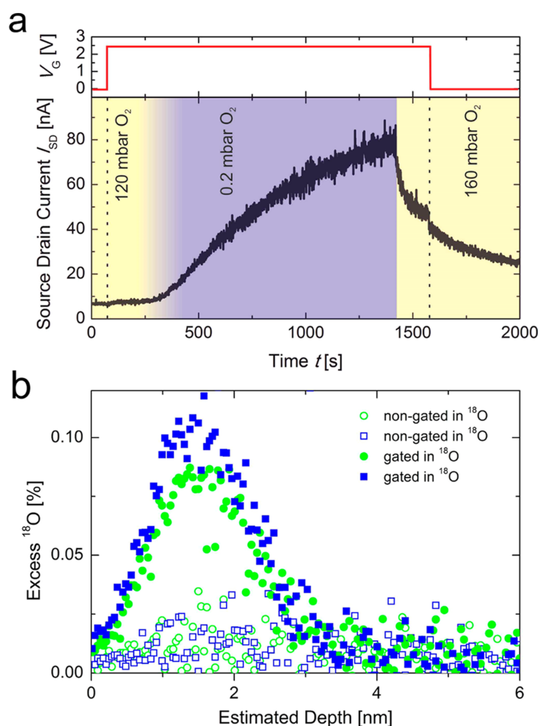

Figure 5. Gating response in oxygen ambient. (a) I_{SD} of a 900 μm × 300 μm device shows negligible gating effect at room temperature in an oxygen pressure of p_{O_2} = 120 mbar with V_G = 2.5 V and V_{SD} = 100 mV. Upon decreasing p_{O_2} gradually to 0.2 mbar, the channel becomes increasingly conductive, evident from an increasing I_{SD}. However, when p_{O_2} was increased abruptly to 160 mbar, a simultaneous decrease in I_{SD} was observed while V_G was maintained at 2.5 V, consistent with the annihilation of oxygen vacancies under high p_{O_2}. When V_G was set to zero, I_{SD} decreased further. (b) Depth dependence of excess ^{18}O concentration over the natural abundance (∼0.2 atomic %) for the same device as in (a) subjected to the same sequence of voltage cycling and $^{18}O_2$ pressure, repeated three times. Depth profiles are shown for two regions within the channel and compared with results from a similar device on the same substrate that was not gated but was subjected to exactly the same dosage of $^{18}O_2$.

0.2 mbar. Furthermore, an immediate drop in I_{SD} occurred when the sample chamber was flooded with oxygen (p = 160 mbar). These results clearly show that an oxygen environment suppresses the I_{SD} response, confirming our thesis that the creation of oxygen vacancies is essential for the gating effect in TiO_2. These experiments strongly suggest that when the IL is saturated with dissolved oxygen the migration path for oxygen from the oxide surface, under the influence of an electric field, into the IL is closed. Oxygen migration out of and into the TiO_2 channel as the device is gated between insulating and conducting states can be detected by labeling the oxygen with ^{18}O. The incorporated oxygen can then be detected using depth profile secondary ion mass spectrometry (SIMS). For these experiments, a TiO_2 device with a large channel area (900 × 300 μm^2) was gated in high vacuum (p < 0.1 mbar, V_G = 2.5 V) to a conducting state. After the channel conductance was saturated,

$^{18}O_2$ (P_{O_2} ~ 120−160 mbar) was introduced into the chamber and V_G was reduced to 0 V. After recovering the insulating state, this procedure of gating the sample in vacuum and introducing $^{18}O_2$ at V_G = 0 V was repeated three times. Figure 5b shows a comparison of the depth profile of ^{18}O, as determined by high-resolution SIMS in two separate 30 μm diameter sized regions, within a gated and a nongated pristine device on the same TiO_2 substrate. Excess ^{18}O over its natural abundance was clearly detected to a depth of ~3.5 nm but only in the gated regions, confirming oxygen vacancy motion during the EDL gating process. These experiments suggest a simple method for distinguishing electrostatic and electrochemical doping effects at oxide surfaces under electrolyte gating by saturating the IL with oxygen.

DISCUSSION

The evidence presented above for the formation of oxygen vacancies under EDL gating also rationalizes the dramatic difference in gating response between (101) and (001) compared to (110) and (100) TiO_2 facets. Not only are the (101) and (001) facets high-energy surfaces and therefore more prone to defect formation, but defects drift faster along the crystallographic [001] direction (*c*-axis)[37] which lies out of plane for (001)- and partly out of plane for (101)-oriented crystals. Our results suggest that the accumulation of vacancies and interstitials at and beyond the surface more readily occurs for (101)- and (001)-oriented samples, consequently forming conducting TiO_{2-x} surfaces. We note that these same high-energy surfaces do not contain the high conductivity axis found in TiO_{2-x} so that the conductivity anisotropy cannot account for the anisotropy in gating response.

CONCLUSIONS

In conclusion, we have provided compelling evidence that electrolyte gating in TiO_2 crystals results from electric-field-induced oxygen vacancy formation that is strongly dependent on the crystal facet orientation. The suppression of any significant gating effect in the presence of pure oxygen furthermore indicates negligible electrostatic gating effects. Recently, related experiments have shown that ionic liquid gating of epitaxial films of VO_2 on both TiO_2 (001) and Al_2O_3 $(10\bar{1}0)$ substrates also leads to the reversible migration of oxygen from the oxide into the ionic liquid with dramatic changes in transport properties.[18] Thus, it is clear that the influence of large electric fields created in electric double layers on modifying the structure of the gated surface or film cannot be ignored. Rather the possibility of modifying the electronic properties of oxides and other materials by the formation of non-equilibrium states is an exciting avenue to novel materials and devices.

METHODS

The devices were fabricated on polished and cleaned single-crystalline rutile TiO_2 substrates with various crystal orientations ((110), (100), (101), and (001), purchased from ARMSC, LLC). Electrodes (5 nm Ta/65 nm Au) in Hall bar geometry were deposited by ion beam evaporation with the TiO_2 surface underneath the electrodes being metalized by Ar ion milling prior to deposition to minimize contact resistance. Amorphous alumina (60 nm) was used to define the channel area (20 × 200 μm) and separate the lateral gate electrode from the TiO_2 surface. Unless otherwise stated in the text, all experiments were carried out using 1-ethyl-3-methylimidazolium bis(trifluoromethylsulfonyl)-imide (EMIM TFSI, EMD Chemicals) as electrolyte. Additionally, 1-hexyl-3-methylimidazolium bis(trifluoromethylsulfonyl)imide (HMIM TFSI, EMD Chemicals) and *N*,*N*-diethyl-*N*-(2-methoxyethyl)-*N*-methylammonium bis(trifluoromethylsulfonyl)imide (DEME TFSI, Sigma-Aldrich) were used as electrolytes. A small droplet of the electrolyte (~0.1 μL) was placed on the device in such a way that it only covered the channel and gate area (see Figure S1). It is known that absorbed water not only can alter the properties of ILs significantly by reducing the electrochemical window but can also dramatically change the performance of EDL FETs by modifying the channel surface.[38] Therefore, all ILs and devices were dried in vacuum (10^{-7} mbar) at 120 °C for 12 h before each experiment. The water content of the ionic liquid measured using ^1H NMR spectroscopy and Karl Fischer titration was well below 50 ppm in a 1 mL sample of IL. The exposure time to air was kept to less than a minute. All electrical measurements were carried out in a DynaCool cryostat (Quantum Design), unless where noted. Transport properties of the TiO_2 EDLTs were measured using Keithley multimeters (2400 and 2002). XPS measurements were done in a vacuum chamber with a base pressure of ~1×10^{-10} mbar with an Al Kα monochromated excitation source of 1486.6 eV incident at an angle of ~78.5°. Spectra were collected with a Thermo VG Alpha-110 hemispherical analyzer at a pass energy of 20 eV collecting photoelectrons emitted normal to the sample surface. A charge compensation gun was used to minimize sample charging during spectra acquisition. IL from the gated samples was rinsed off with isopropyl alcohol before acquiring the XPS spectra. EDL gating experiments in the presence of $^{18}O_2$ were performed in a vacuum chamber with a base pressure of 10^{-7} mbar. Prior to each experiment, the sample was heated to 120 °C and pumped for several hours and then backfilled with ultrapure $^{18}O_2$ (Sigma-Aldrich).

SIMS was carried out using a CAMECA SC Ultra instrument. A 3 nm thick Pt film was deposited on the sample to reduce charging effects. A 30 μm diameter beam of 600 eV Cs^+ ions was rastered over a ~300 × 300 μm^2 region within the channel to create a crater. SIMS data were collected within a central 30 μm diameter region with a mass resolution sufficient to clearly resolve ^{18}O from $^{16}O^1H_2$ and $^{17}O^1H$.

Conflict of Interest: The authors declare no competing financial interest.

Acknowledgment. T.S. thanks the Alexander von Humboldt Foundation for a Feodor Lynen Research Fellowship, and T.G. is a recipient of a stipend from the German Science foundation (DFG, GR4000/1-1). Support from the Graduate School "Material Science in Mainz" (DFG, GSC 266) is also gratefully acknowledged. We also thank C. Felser for discussions, V. Deline for the SIMS measurements, B. Hughes for help with device fabrication, and members of the Army Research Office supported Oxide MURI for useful discussions.

Supporting Information Available: Device schematic, electronic transport characteristics of TiO_2 (101) samples, electronic

transport in EDL-gated TiO_2 (001), and low-temperature transport theory. This material is available free of charge *via* the Internet at http://pubs.acs.org.

REFERENCES AND NOTES

1. Ahn, C. H.; Bhattacharya, A.; Di Ventra, M.; Eckstein, J. N.; Frisbie, C. D.; Gershenson, M. E.; Goldman, A. M.; Inoue, I. H.; Mannhart, J.; Millis, A. J.; *et al.* Electrostatic Modification of Novel Materials. *Rev. Mod. Phys.* **2006**, *78*, 1185–1128.
2. Taur, Y.; Ning, T. H. *Fundamentals of Modern Vlsi Devices*; Cambridge University Press: Cambridge, UK, 1998.
3. Okamoto, S.; Millis, A. J. Electronic Reconstruction at an Interface between a Mott Insulator and a Band Insulator. *Nature* **2004**, *428*, 630–633.
4. Moetakef, P.; Cain, T. A.; Ouellette, D. G.; Zhang, J. Y.; Klenov, D. O.; Janotti, A.; Van de Walle, C. G.; Rajan, S.; Allen, S. J.; Stemmer, S. Electrostatic Carrier Doping of $GdTiO_3/SrTiO_3$ Interfaces. *Appl. Phys. Lett.* **2011**, *99*, 232116-4.
5. Reyren, N.; Thiel, S.; Caviglia, A. D.; Kourkoutis, L. F.; Hammerl, G.; Richter, C.; Schneider, C. W.; Kopp, T.; Ruetschi, A. S.; Jaccard, D.; *et al.* Superconducting Interfaces between Insulating Oxides. *Science* **2007**, *317*, 1196–1199.
6. Mannhart, J.; Schlom, D. G. Oxide Interfaces—An Opportunity for Electronics. *Science* **2010**, *327*, 1607–1611.
7. Singh-Bhalla, G.; Bell, C.; Ravichandran, J.; Siemons, W.; Hikita, Y.; Salahuddin, S.; Hebard, A. F.; Hwang, H. Y.; Ramesh, R. Built-in and Induced Polarization across $LaAlO_3/SrTiO_3$ Heterojunctions. *Nat. Phys.* **2010**, *7*, 80–86.
8. Gunkel, F.; Brinks, P.; Hoffmann-Eifert, S.; Dittmann, R.; Huijben, M.; Kleibeuker, J. E.; Koster, G.; Rijnders, G.; Waser, R. Influence of Charge Compensation Mechanisms on the Sheet Electron Density at Conducting $LaAlO_3/SrTiO_3$-Interfaces. *Appl. Phys. Lett.* **2012**, *100*, 052103-3.
9. Bark, C. W.; Sharma, P.; Wang, Y.; Baek, S. H.; Lee, S.; Ryu, S.; Folkman, C. M.; Paudel, T. R.; Kumar, A.; Kalinin, S. V.; *et al.* Switchable Induced Polarization in $LaAlO_3/SrTiO_3$ Heterostructures. *Nano Lett.* **2012**, *12*, 1765–1771.
10. Yamamoto, R.; Bell, C.; Hikita, Y.; Hwang, H. Y.; Nakamura, H.; Kimura, T.; Wakabayashi, Y. Structural Comparison of n-Type and p-Type $LaAlO_3/SrTiO_3$ Interfaces. *Phys. Rev. Lett.* **2011**, *107*, 036104.
11. Ueno, K.; Nakamura, S.; Shimotani, H.; Ohtomo, A.; Kimura, N.; Nojima, T.; Aoki, H.; Iwasa, Y.; Kawasaki, M. Electric-Field-Induced Superconductivity in an Insulator. *Nat. Mater.* **2008**, *7*, 855–858.
12. Bollinger, A. T.; Dubuis, G.; Yoon, J.; Pavuna, D.; Misewich, J.; Bozovic, I. Superconductor−Insulator Transition in $La_{2-x}Sr_xCuO_4$ at the Pair Quantum Resistance. *Nature* **2011**, *472*, 458–460.
13. Ye, J. T.; Inoue, S.; Kobayashi, K.; Kasahara, Y.; Yuan, H. T.; Shimotani, H.; Iwasa, Y. Liquid-Gated Interface Superconductivity on an Atomically Flat Film. *Nat. Mater.* **2010**, *9*, 125–128.
14. Yamada, Y.; Ueno, K.; Fukumura, T.; Yuan, H. T.; Shimotani, H.; Iwasa, Y.; Gu, L.; Tsukimoto, S.; Ikuhara, Y.; Kawasaki, M. Electrically Induced Ferromagnetism at Room Temperature in Cobalt-Doped Titanium Dioxide. *Science* **2011**, *332*, 1065–1067.
15. Yuan, H.; Shimotani, H.; Tsukazaki, A.; Ohtomo, A.; Kawasaki, M.; Iwasa, Y. High-Density Carrier Accumulation in ZnO Field-Effect Transistors Gated by Electric Double Layers of Ionic Liquids. *Adv. Funct. Mater.* **2009**, *19*, 1046–1053.
16. Sato, T.; Masuda, G.; Takagi, K. Electrochemical Properties of Novel Ionic Liquids for Electric Double Layer Capacitor Applications. *Electrochim. Acta* **2004**, *49*, 3603–3611.
17. Galiński, M.; Lewandowski, A.; Stępniak, I. Ionic Liquids as Electrolytes. *Electrochim. Acta* **2006**, *51*, 5567–5580.
18. Jeong, J.; Aetukuri, N.; Graf, T.; Schladt, T. D.; Samant, M. G.; Parkin, S. S. P. Suppression of Metal−Insulator Transition in VO_2 by Electric Field-Induced Oxygen Vacancy Formation. *Science* **2013**, *339*, 1402–1405.
19. Lee, P. A.; Ramakrishnan, T. V. Disordered Electronic Systems. *Rev. Mod. Phys.* **1985**, *57*, 287–337.
20. Becker, J. H.; Hosler, W. R. Multiple-Band Conduction in n-Type Rutile (TiO_2). *Phys. Rev.* **1965**, *137*, A1872–A1877.
21. Yagi, E.; Hasiguti, R. R.; Aono, M. Electronic Conduction above 4 K of Slightly Reduced Oxygen-Deficient Rutile TiO_{2-x}. *Phys. Rev. B* **1996**, *54*, 7945–7956.
22. Diebold, U. The Surface Science of Titanium Dioxide. *Surf. Sci. Rep.* **2003**, *48*, 53–229.
23. Ramamoorthy, M.; Vanderbilt, D.; King-Smith, R. D. First-Principles Calculations of the Energetics of Stoichiometric TiO_2 Surfaces. *Phys. Rev. B* **1994**, *49*, 16721–16727.
24. Linsebigler, A. L.; Lu, G.; Yates, J. T. Photocatalysis on TiO_2 Surfaces: Principles, Mechanisms, and Selected Results. *Chem. Rev.* **1995**, *95*, 735–758.
25. Hollander, L. E., Jr.; Castro, P. L. Anisotropic Conduction in Nonstoichiometric Rutile (TiO_2). *Phys. Rev.* **1960**, *119*, 1882–1885.
26. Morgan, B. J.; Watson, G. W. A Density Functional Theory + U Study of Oxygen Vacancy Formation at the (110), (100), (101), and (001) Surfaces of Rutile TiO_2. *J. Phys. Chem. C* **2009**, *113*, 7322–7328.
27. Dong, K.; Zhang, S.; Wang, D.; Yao, X. Hydrogen Bonds in Imidazolium Ionic Liquids. *J. Phys. Chem. A* **2006**, *110*, 9775–9782.
28. Zheng, W.; Liu, X.; Yan, Z.; Zhu, L. Ionic Liquid-Assisted Synthesis of Large-Scale TiO_2 Nanoparticles with Controllable Phase by Hydrolysis of $TiCl_4$. *ACS Nano* **2009**, *3*, 115–122.
29. Yaghi, O. M.; Li, G.; Li, H. Selective Binding and Removal of Guests in a Microporous Metal-Organic Framework. *Nature* **1995**, *378*, 703–706.
30. Zhao, X.; Jin, W.; Cai, J.; Ye, J.; Li, Z.; Ma, Y.; Xie, J.; Qi, L. Shape- and Size-Controlled Synthesis of Uniform Anatase TiO_2 Nanocuboids Enclosed by Active {100} and {001} Facets. *Adv. Funct. Mater.* **2011**, *21*, 3554–3563.
31. Lockett, V.; Sedev, R.; Ralston, J.; Horne, M.; Rodopoulos, T. Differential Capacitance of the Electrical Double Layer in Imidazolium-Based Ionic Liquids: Influence of Potential, Cation Size, and Temperature. *J. Phys. Chem. C* **2008**, *112*, 7486–7495.
32. Jeong, D. S.; Schroeder, H.; Waser, R. Mechanism for Bipolar Switching in a $Pt/TiO_2/Pt$ Resistive Switching Cell. *Phys. Rev. B* **2009**, *79*, 195317.
33. Umecky, T.; Saito, Y.; Matsumoto, H. Direct Measurements of Ionic Mobility of Ionic Liquids Using the Electric Field Applying Pulsed Gradient Spin−Echo NMR. *J. Phys. Chem. B* **2009**, *113*, 8466–8468.
34. Cho, J. H.; Lee, J.; He, Y.; Kim, B.; Lodge, T. P.; Frisbie, C. D. High-Capacitance Ion Gel Gate Dielectrics with Faster Polarization Response Times for Organic Thin Film Transistors. *Adv. Mater.* **2008**, *20*, 686–690.
35. Sayers, C. N.; Armstrong, N. R. X-ray Photoelectron Spectroscopy of TiO_2 and Other Titanate Electrodes and Various Standard Titanium Oxide Materials: Surface Compositional Changes of the TiO_2 Electrode during Photoelectrolysis. *Surf. Sci.* **1978**, *77*, 301–320.
36. Silversmit, G.; Depla, D.; Poelman, H.; Marin, G. B.; De Gryse, R. Determination of the V 2p XPS Binding Energies for Different Vanadium Oxidation States (V^{5+} to V^{0+}). *J. Electron Spectrosc. Relat. Phenom.* **2004**, *135*, 167–175.
37. Jameson, J. R.; Fukuzumi, Y.; Wang, Z.; Griffin, P.; Tsunoda, K.; Meijer, G. I.; Nishi, Y. Field-Programmable Rectification in Rutile TiO_2 Crystals. *Appl. Phys. Lett.* **2007**, *91*, 112101-3.
38. Yuan, H.; Shimotani, H.; Tsukazaki, A.; Ohtomo, A.; Kawasaki, M.; Iwasa, Y. Hydrogenation-Induced Surface Polarity Recognition and Proton Memory Behavior at Protic-Ionic-Liquid/Oxide Electric-Double-Layer Interfaces. *J. Am. Chem. Soc.* **2010**, *132*, 6672–6678.